International Journal of GEOMATE, Jan., 2024 Vol.26, Issue 113, pp.107-114
ISSN: 2186-2982 (P), 2186-2990 (O), Japan, DOI: https://doi.org/10.21660/2024.113.g13367
Geotechnique, Construction Materials and Environment

QUANTIFYING THE SURFACE ROUGHNESS EVALUATION OF RAILWAY BALLAST GRAIN UNDER ROTATING DRUM ABRASION

Opu Chandra Debanath[1,2], Takashi Matsushima[1]*, Shuichi Adachi[3] and Masahiro Miwa[3]

[1]Department of Engineering Mechanics and Energy, University of Tsukuba, Japan;
[2]Department of Civil Engineering, Chittagong University of Engineering & Technology, Bangladesh;
[3]Central Japan Railway Company, Komaki, Japan

*Corresponding Author, Received: 14 June 2023, Revised: 24 Nov. 2023, Accepted: 15 Dec. 2023

ABSTRACT: Railway ballast is a crucial component of the railway infrastructure, with the geometric shape and surface morphology of ballast grains playing an essential role in the overall strength of the ballasted track. This study investigates the evolution of surface roughness for two types of railway ballast, Andesite and Sandstone, at various stages of abrasion using a rotating drum test. The surface texture changes are analyzed by comparing amplitude roughness parameters and power spectral density distributions. Additionally, the overall grain shape change is tracked by grain shape parameters: ellipsoid volume ratio and rotation resistance angle. A 3D scanning workflow is developed using the focus stacking method; the accuracy is verified by standard surface S-22. Experimental findings reveal that laboratory-abraded ballast grains exhibit significantly lower roughness than fresh ballast grains, following a power law decay with abrasion cycles. Notably, roughness does not differ substantially between the Andesite and Sandstone ballast. The observed surface roughness evolution is attributed to the progressive removal of surface peaks through continuous attrition at the interfaces between grains and the drum wall. Furthermore, the study reveals that the abrasion process primarily involves the removal of surface texture, followed by subsequent changes in angularity and overall grain shape.

Keywords: Railway ballast, Surface roughness, Grain abrasion, Power spectral density

1. INTRODUCTION

In railway infrastructure, ballasted track systems are widely adopted for their load transmission and dissipation capabilities. Ballast is composed of crushed rock, which typically ranges from 25 mm to 65 mm in size. The primary role of the ballast layer is to transfer and dissipate the loads from moving trains to the underlying subgrade layer. As trains continuously move, the ballast particles experience degradation under repeated cyclic load, often identified as a primary factor leading to differential track settlement, subgrade pumping, and other issues. Consequently, maintenance and ballast replacement become necessary when the materials degrade beyond a certain threshold [1, 2]. Therefore, understanding and accurately estimating this degradation process is a crucial aspect of railway infrastructure management.

Previous researchers have experimentally examined the degradation of ballast material and its influence on mechanical strength. The experimental degradation of ballast is quantified by the bulk degradation of materials such as fowling index, relative breakage, and ballast breakage index [3–5]. However, the degradation of bulk assembly greatly depends on the shape change of individual grains. Considering this issue, recent research on ballast materials has focused on the evolution of grain size, shape, and angularity due to abrasion [6–9]. The change of grain shape indices, such as flakiness, elongation, sphericity, convexity, etc., assesses the grain-scale degradation. Although grain shape and angularity are still active research topics, the study of surface roughness is one step ahead of understanding the microscopic contact-scale behavior of ballast particles. Among many other engineering applications, including contact resistance of metal surfaces, wear, contact friction, and joint rock strength [10–12], the study of surface roughness characteristics is equally important for railway ballast grains. This is because the roughness of individual grain surfaces affects the interparticle friction coefficient, normal stiffness, and shear modulus [13]. Ballast particles undergo continuous attrition throughout their lifespan primarily due to grain-to-grain sliding, which gradually changes surface roughness. Thus, monitoring ballast grains' surface morphology at different degradation stages is also necessary. However, comprehensive studies are lacking to describe the evolution of surface roughness and overall grain shape under continuous abrasion.

In this study, we attempt to characterize the surface topography of fresh railway ballast and laboratory-abraded ballast grains. The accelerated degradation of ballast is induced by the rotating drum abrasion test. We first developed a simple workflow to scan the ballast surface using a microscope and focus stacking algorithm. The surface topography of selected grains was recorded periodically to capture the transformation of surface topography. In addition, the overall grain shape is also recorded. Finally, the

evolution of surface roughness is described in terms of amplitude roughness parameters and power spectral density. Consequently, the evolution of overall shape is described in terms of grain form and angularity. The mechanism of ballast degradation is identified as a continuous process, beginning with the removal of surface texture and subsequently followed by grain form and angularity changes.

2. RESEARCH SIGNIFICANCE

The study of ballast materials is vital for railway construction and management. Individual ballast grains play a significant role in bulk assembly, and the morphological analysis of ballast grain is important. While the previous research focused on the evolution of the overall form of ballast grains, this study is one step ahead in tracking the microscopic surface roughness change during the abrasion. Additionally, the grain shape vs roughness evolution contributes to describing the multi-scale evolution of ballast grains during experimental abrasion.

3. EXPERIMENTAL CAMPAIGN

This study tracks the surface roughness evolution during experimental abrasion. We used an accelerated experiment using a rotating drum, and grain surface scanning was also done simultaneously. The following subsections describe the details of experimental procedures.

3.1 3D Surface Scanning

A wide range of surface scanning methods [14–16] is available nowadays, including scanning electron microscopy, atomic force microscopy, white light scanning interferometry, and laser scanning, directly providing the 3D profile output. In the current experimental program, we developed a workflow to scan ballast surfaces using a reflected light microscope and focus stacking.

Focus stacking [17], also known as z-stacking or focal plane merging, is a technique to create images with greater depth of field. It involves capturing multiple images with different focus points and combining them to create a final image with all parts of the subject in sharp focus. A confocal microscope (Olympus BX51M) equipped with a camera mount port was used to capture 2D photographs. The objective lens magnification was kept constant at 20x throughout the study, and an SLR camera (canon Kiss X7) was mounted to the C-mount video camera adapter (U-TV1x-2). In addition, the microscope was assembled with a z-axis drive controller (MFC-2000) that enables precise focus control. A series of 2D photographs were first captured at different focal lengths. Then, we used a commercially available software helicon focus for stacking the images.

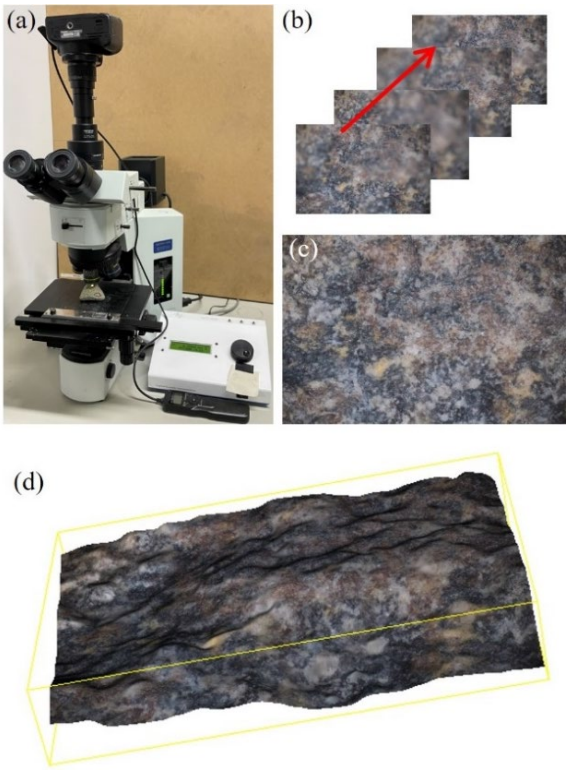

Fig.1 Focus stacking workflow: (a) microscope setup, (b) image stack having different focus point, (c) final image after stacking, and (d) reconstructed 3D surface topography

The captured image was first imported into the workspace. The focused area of each image was identified and subsequently merged to reconstruct an image with full focus. Alongside this, a depth map of the image was simultaneously constructed and employed to generate a 3D representation of the surface topography. Fig.1 illustrates the microscope setup and 3D reconstruction process. The selection of an optimum number of photographs depends on surface irregularity; however, there is no specific threshold for reconstruction. Too few images in the stack will lead to surface information being lost, as portions of the final merged image will remain blurry. In the current workflow, we used 20 to 30 photographs for each stacking to reconstruct the entire surface.

3.2 Measurement of Standard Surface

The accuracy of the 3D scanning method is checked by comparing the roughness values of standard machine-finished surfaces. A commercially available surface comparator, GAR S-22, was used in the current study.

The micro-finish comparator contains 22 types of machine finishes having specific patterns and roughness values. We scanned the surfaces designated as 63ST, 125ST, 250ST, and 500ST,

marked red in Fig.2 (a). The numeric values represent the standard average roughness height in the micro-inch unit. The suffix ST stands for the shape-turned surface texture that lays are parallel to the specimen's long dimension. Fig.2 (b) shows an example three-dimensional plot of surface 125ST.

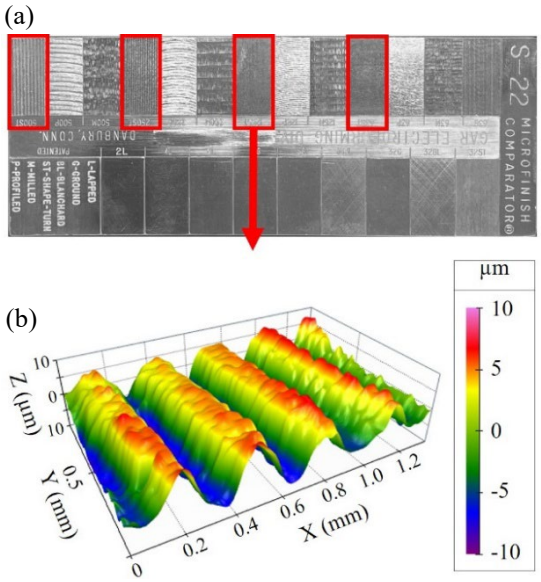

Fig.2 (a) S-22 Micro-finish surface comparator, and (b) 3D profile of the surface 125ST

We scanned at random points over the surface for each selected texture, and the arithmetic average of 30 observations was reported as a roughness value for each case. The average surface roughness values of shape-turned surfaces scanned by the focus stacking method are plotted in Fig. 3.

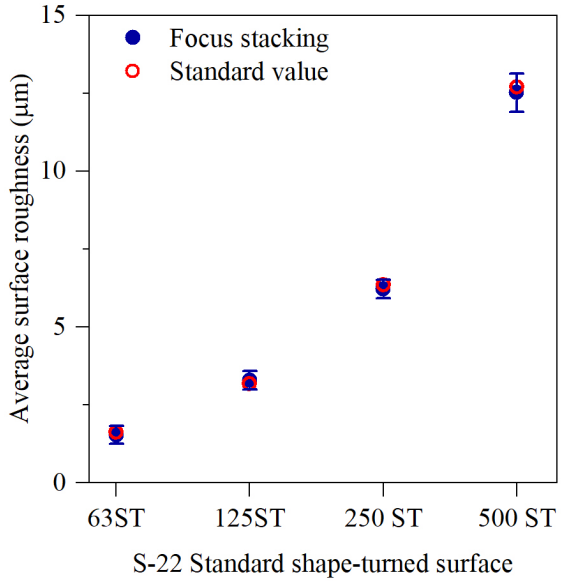

Fig.3 Average roughness of shape-turned surface measured by focus stacking method

The S-22 surface roughness comparator provides reported surface roughness values for 63ST, 125ST, 250ST, and 500ST finishes as 1.60, 3.18, 6.35, and 12.7 µm, respectively, within tolerance limits of 15–20%[18, 19]. The average roughness values measured by the focus stacking method closely match standard values, and the standard deviations lie within the tolerance range.

3.3 Abrasion Test

We conducted a rotating drum test to abrade ballast grain in the current experimental campaign. The test assembly comprised 7.0 kg of ballast materials consisting of 75-100 grains with a size range of 25-50 mm, placed inside a cylindrical drum with an inner diameter of 30 cm and a depth of 25 cm and rotated at a constant speed of 70 rpm. The abrasion test was performed for two types of railway ballast materials: Andesite and Sandstone. The test was interpreted at varying abrasion cycles to record the necessary data. In addition to surface scanning over specific patches, the overall grain geometry was also scanned. The photogrammetric reconstruction method was adopted for the 3D scanning of ballast grain; the details of the drum test and ballast scanning are explained in [20]. The examining ballast grains were marked by color for ease of isolation from the bulk assembly.

A series of surface patches distributed widely over the grain surface was scanned periodically; several specific patches were marked for comparison. However, the selection of surface patches is based on the judgment of ease placement under the microscope lens depending on grain geometry.

Fig.4 A view of fresh (before) and abraded (after) ballast grains 96,000 abrasion cycles

4. RESULT AND DISCUSSION

4.1 Evolution of Surface Roughness

4.1.1 Amplitude roughness parameter

In the current study, we adopted amplitude parameters, the most common approach to describing roughness characteristics of surface topography [21–23]. We considered the following scaler parameters to explain the roughness evolution of ballast surfaces: Spatial root-mean-square roughness (S_q) and Maximum peak-to-valley height (R_zJIS). The first

parameter, RMS roughness (Eq.1), represents the root mean square of height deviations from the mean surface level. Where $Z(x_i y_j)$ is the height deviation of the ij[th] surface points, and m and n denote the number of points along the x and y directions. R_zJIS, another roughness parameter defined by the Japanese Industrial Standard (Eq.2), is computed as the average sum of the five highest peaks and the five lowest valleys within the surface profile, where Z_{pi} and Z_{pi} are the i[th] highest peak and lowest valley, respectively.

$$S_q = \sqrt{\frac{1}{mn}\sum_{i=1}^{m}\sum_{j=1}^{n}[Z(x_i y_j)]^2} \quad (1)$$

$$R_z JIS = \frac{1}{5}\sum_{i=1}^{5}(Z_{pi} + Z_{vi}) \quad (2)$$

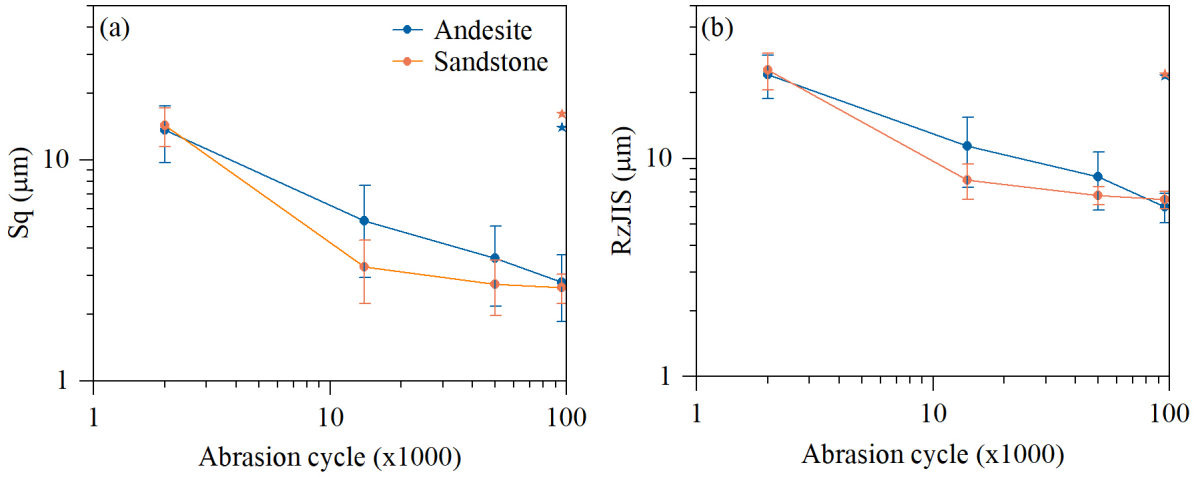

Fig.5 Evolution of amplitude parameters in log-log plot: (a) RMS roughness and (b) peak-to-valley roughness. The error bar denotes the minimum-maximum range, with (●) indicating the mean value; the (★) markers represent the average roughness of the concave region at the end of the abrasion

Fig. 5 (a-b) illustrates the evolution of root means square roughness and peak-to-valley distance against progressive abrasion cycles in a logarithmic scale. Considering that the concave points of the grain surface have a lower probability of abrasion than the convex regions, selected concave surface patches were only scanned at the end of the abrasion test. The star markers represent the average values of these concave points after 96000 revs.

The following observations can be derived from the amplitude parameter results. Firstly, no significant difference between measured roughness values can be seen when comparing the Andesite and Sandstone ballast. Secondly, the initial roughness data display a high degree of scatter; the Sq value of fresh ballast surface varies between 12.5 - 24.7 μm, and the RzJIS varies between 24.4 - 37.7 μm, respectively. The average RMS roughness of granite ballast was reported as 17 μm [24].

Thirdly, the roughness parameters evolve gradually with the abrasion cycle, demonstrating a power law decay of surface roughness. At 96000 revs., the average Sq and RzJIS values are 2.7 μm and 6.2 μm, respectively, representing a reduction of three to seven times compared to the initial roughness values. It is important to note that the microscope used in this study has a minimum patch movement of 0.005mm, limiting its accuracy in capturing beyond the micron scale, and the test is stopped hereafter. Fig.6 (a-e) depicts the 3D profile of a surface patch at various stages of abrasion.

It is evident that the sharp peaks on the ballast surface gradually diminish as the abrasion proceeds and turns to a regular texture. However, the concave surface points, which have a lower probability of contact, exhibit an unchanged surface texture, as evidenced by the roughness values at the end of the test, denoted by the star markers in the plot and the 3D profile (Fig.6 f).

4.1.2 Spectral Density Analysis

The Power spectral density (PSD) is a statistical measure widely used [25–27] to analyze the distribution of roughness intensity. It describes how the surface roughness power is distributed over different spatial frequencies. Eq. 3 shows the computation of spectral density. Where C^{2D} is the spectral density in surface across q_x and q_y, the measured wavenumber is q (the corresponding wavelength is given by $L = 2\pi/q$). Given the aperiodic nature of the ballast surface, it was necessary to impose periodicity before the PSD analysis, achieved by processing the surface height data using the Welch window method [28].

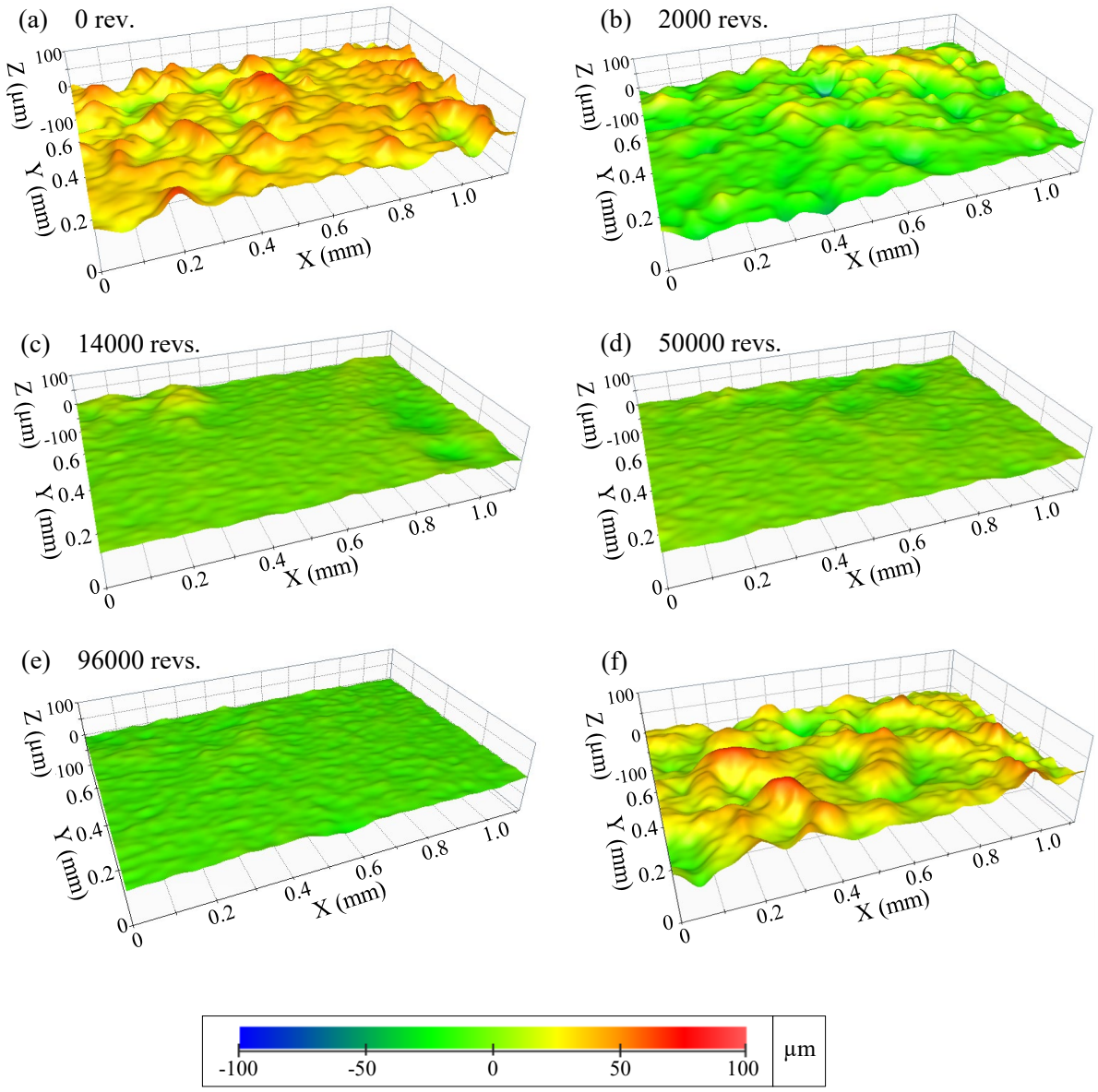

Fig.6 (a-e) Topographical profile of grain surface at incremental abrasion cycle, and (f) one concave point of grain surface after 96000 revs.

$$h_{rms}^2 = \frac{1}{(2\pi)^2} \iint_{-\infty}^{\infty} C^{2D}(q_x q_y)\, dq_x dq_y \qquad (3)$$

Fig. 7 depicts the power spectral density curve of a specific surface patch on a ballast grain at increasing drum rotation. It is seen that the fresh ballast surface exhibits a greater density of surface texture across the wavenumber compared to the rotating drum-abraded ballast surfaces, and a gradual loss of surface roughness is observed throughout the abrasion cycle.

4.2 Evolution of Grain Shape

Damage to ballast grains can occur at various scales, ranging from millimeters to micrometers. The overall shape and angularity of grains govern the coarse-scale interlocking between ballast particles, whereas surface roughness plays a crucial role in influencing inter-particle friction. Therefore, it is necessary to understand the relationship between ballast shape and surface roughness. In the current study, we adopted the following shape parameters: a) ellipsoid volume ratio (e_v) and b) the rotational resistance angle (α_p). The first parameter represents the overall grain form, while the latter indicates the angularity. These parameters are computed from the 3D model of the ballast grain captured at the incremental stage of the abrasion cycle. Fig. 8(a) shows the geometric representation of an equivalent ellipsoid over a ballast particle. Correspondingly, Fig. 8(b) demonstrates the computation of the rotational

resistance angle. Mathematical expressions of these two parameters are given in Eq. 4-5. The e_v is computed as the volume ratio of the original grain to a best-fit ellipsoid. The best-fitted ellipsoid is generated for the 3D ballast model so that the three principal moments of inertia are identical to those of the original grain.

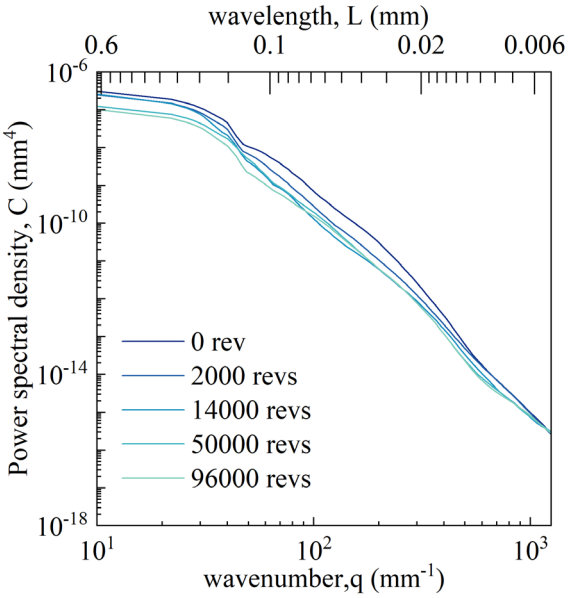

Fig.7 Evolution of PSD curve over a specific patch of grain surface at increasing abrasion cycle

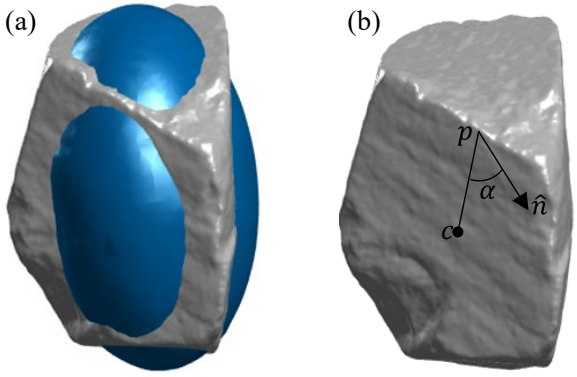

Fig.8 Illustration of grain shape parameters: (a) ellipsoid volume ratio, ev; and (b) rotational resistance angle, α_p

$$e_v = \frac{V}{V_{ellipsoid}} \quad (4)$$

$$\alpha_p = \frac{1}{A}\int \alpha \, dS \quad (5)$$

The value of the ellipsoid volume ratio is smaller than unity when the particle shape deviates more from the ellipsoid shape. The typical value of e_v lies within the range of 0.93 to 0.98 for fresh ballast particles. Another parameter, α_p, is a mechanics-based shape index originally proposed by Kawamoto et al. [29] representing the angularity, and the value of α_p *is* 0 for a spherical particle. At any surface point of a 3D mesh, the angle α represents the deviation between the surface normal at that specific point and the radial vector connecting the point to the particle centroid line. The variable *dS* denotes the area of the triangular face associated with the point. The rotational resistant angle, αp, is then computed by determining the weighted average of α across the entire particle surface, where *A* represents the total surface area of the mesh.

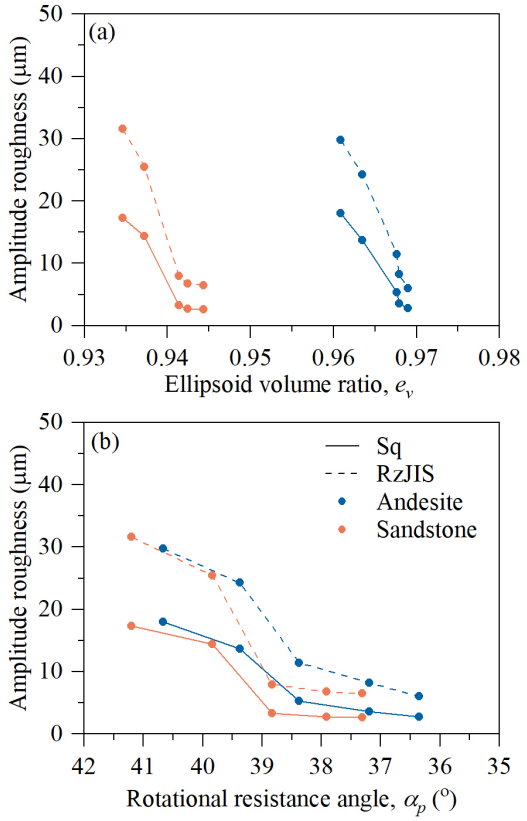

Fig.9 Relation between overall grain shape and surface roughness: (a) ellipsoid volume ratio, and (b) rotational resistance angle.

Fig.9 illustrates the surface roughness alongside the overall grain shape. The average values of amplitude roughness parameters at the incremental abrasion cycle are plotted against the grain shape parameters. The solid line in the figure represents the root mean square roughness values (Sq), while the dashed line corresponds to the Peak-to-Valley distance (RzJIS), with the circular markers showing mean values. The ellipsoid volume ratio shows minimal change as abrasion progresses. The initial e_v values for the fresh grain were 0.960 and 0.935 for Andesite and Sandstone, respectively, and these

values changed to 0.969 and 0.945 at the end of the abrasion process. On the other hand, the rotational resistance angle (αp) decreases significantly, from 40.7° to 36.4° for Andesite and from 41.2° to 37.3° for Sandstone grain. This observation indicates that the grain shape remains unchanged while the angularity changes during abrasion.

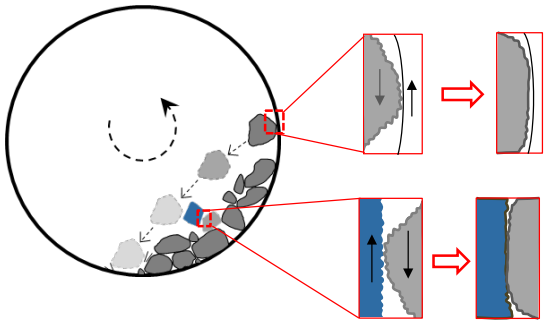

Fig.10 Attrition mechanism during the rotating drum abrasion

According to the experimental findings described above, the grain abrasion mechanism can be defined as a continuous process of attrition, which primarily contributes to the decrease in ballast roughness. The attrition inside the rotating drum mainly occurs due to grain-to-grain and grain-to-wall interactions [30]. Fig. 10 schematically illustrates the attrition mechanism during the abrasion process, depicting the consequential change in surface texture. When two neighboring grains come into contact, their convex regions are sheared against each other.

At the same time, grain-to-wall attrition involves the ballast surfaces being sheared against a relatively flat metal surface. Such repeated shearing process removes micro-texture from the grain surface, reflected as a reduction of surface roughness. Furthermore, the abrasion of local corners and edges contributes to the evolution of angularity, while the overall grain form remains unchanged throughout the abrasion.

5. CONCLUSION

This study quantitatively explored the evolution of surface roughness of two types of railway ballast: Andesite and Sandstone, during various stages of abrasion under a rotating drum test. The transformation of surface texture was characterized via amplitude roughness parameters and power spectral density analysis, along with an assessment of overall grain shape. The findings indicate that laboratory-abraded ballast grains have significantly lower roughness than fresh ones. The fresh ballast grains exhibit a wide range of roughness distribution that decreases sharply at the initial stage and levels off afterward. Interestingly, no significant roughness difference between Andesite and Sandstone ballasts was identified. The findings suggest that the abrasion process primarily involves the removal of surface texture, followed by changes in angularity and overall grain form.

While this study reports on the roughness evolution during abrasion, future research is expected to investigate the relationship between the interparticle friction and the surface roughness of ballast grains.

6. ACKNOWLEDGMENTS

The authors deeply appreciate the financial support grants from the Japanese government scholarship MEXT. The authors also want to thank JR Central for supplying the test materials.

7. REFERENCES

[1] Abadi T., Madhusudhan B.N., Li H., Le Pen L., Reusing Life-Expired Railway Ballast: Laboratory Testing, Shape Analysis, and Petrographic Evaluation. Journal of Geotechnical and Geoenvironmental Engineering, Vol. 149, Issue 1, 2023.

[2] Kim J., Park B. S., Woo S. I., Choi Y. T., Evaluation of ballasted-track condition based on aggregate-shape characterization. Construction and Building Materials, Vol. 232, 2020, pp. 1-9.

[3] Koohmishi M., Palassi M., Degradation of railway ballast under impact loading considering the morphological properties of aggregate. Transportation Geotechnics, Vol. 25, 2020, pp. 1-13.

[4] Fathali M., Chalabii J., Astaraki F., Esmaeili M., A new degradation model for life cycle assessment of railway ballast materials. Construction and Building Materials, Vol. 270, 2021.

[5] Bian X., Shi K., Li W., Luo X., Tutumluer E., Chen Y., Quantification of Railway Ballast Degradation by Abrasion Testing and Computer-Aided Morphology Analysis. Journal of Materials in Civil Engineering, Vol. 33, Issue 1, 2021.

[6] Czinder B., Vásárhelyi B., Török Á., Long-term abrasion of rocks assessed by micro-Deval tests and estimation of the abrasion process of rock types based on strength parameters. Engineering Geology, Vol. 282, 2021.

[7] Liu J., Zhao S., Mullin A., Laboratory assessment of Alaska aggregates using Micro-Deval test. Frontiers of Structural and Civil Engineering, Vol. 11, 2017, pp.27-34.

[8] Lane D.S., Druta C., Wang L., Xue, W., Modified micro-Deval procedure for evaluating the polishing tendency of coarse aggregates. Transportation research record, Vol. 2232, Issue 1, 2011, pp.34-43.

[9] Qian Y., Tutumluer E., Hashash Y.M., Ghaboussi J., Triaxial testing of new and degraded ballast under dry and wet conditions. Transportation Geotechnics, Vol. 34, 2022.
[10] Wang F., Wang S., Yao W., Li X., Meng F., Xia K., Effect of roughness on the shear behavior of rock joints subjected to impact loading. Journal of Rock Mechanics and Geotechnical Engineering, Vol. 15, Issue 2, 2023, pp. 339-349.
[11] Cui C., Gratchev I., Chung M., Kim D. H., Changes in joint surface roughness of two natural rocks during shearing. International Journal of GEOMATE, Vol. 17, Issue 63, 2019, pp. 181-186.
[12] Jayabarathi S. B., Ratnam M. M., Correlation Study of 3D Surface Roughness of Milled Surfaces with Laser Speckle Pattern. Sensors, Vol. 22, Issue 8, 2022, pp. 1-16.
[13] Nadimi S., Angelidakis V., Otsubo M., Ghanbarzadeh A., How can the effect of particle surface roughness on the contact area be predicted? Computers and Geotechnics, Vol. 150, 2022.
[14] Wongkaew B., Wongkaew P., Thanutong P., Thanutong C., Nanostructural characterization of glutathione-S-transferase immobilizing Chitosan modified screen printed carbon electrode by atomic force microscopy. International Journal of GEOMATE, Vol. 14, Issue 43, 2018, pp. 132-139.
[15] Wongkaew P., Poosittisak S., Atomic Force Microscopic and Electrochemical Characterization of the Modified Screen Printed Carbon Electrode by Self Assembled Deposition of Chitosan and Activated Carbon. International Journal of GEOMATE, Vol. 11, Issue 24, 2016, pp. 2356-2362.
[16] Mah J., Samson C., McKinnon S.D., Thibodeau D., 3D laser imaging for surface roughness analysis. International Journal of Rock Mechanics and Mining Sciences, Vol. 58, 2013, pp.111-117.
[17] Wlodek J., Gofron K.J., Cai Y.Q., Achieving 3D imaging through focus stacking. In AIP Conference Proceedings, Vol. 2054, Issue 1, 2019.
[18] ASME B46.1, Surface Texture, Surface Roughness, Waviness and Lay. 2009, pp. 68-75.
[19] Said M., Eng C.W., Hixon A.E., Marks N.E., Quantifying surface roughness on UO_2 fuel pellets using optical techniques. Forensic Science International, Vol. 316, 2020.
[20] Debanath O. C., Matsushima T., Ijichi T., Miwa M., Morphological Evolution of Andesite Railway Ballast Particle under Rotating Drum Abrasion Test. in Proc. 6th ICACE, 2022, pp. 407-415.
[21] Gadelmawla E. S., Koura M. M., Maksoud T. M. A., Elewa I. M., Soliman H. H., Roughness parameters. Journal of Materials Processing Technology, Vol. 123, 2002, Issue 1, pp. 133-145.
[22] Deltombe R., Kubiak K.J. and Bigerelle M., How to select the most relevant 3D roughness parameters of a surface. Scanning. The Journal of Scanning Microscopies, Vol. 36, Issue 1, 2014, pp. 150-160.
[23] Han J., Zheng W., Chen Q., Sun J., Xu S., Study on size effect of surface roughness based on the 3D Voronoi model and establishment of roughness prediction model in micro-metal forming. Coatings, Vol. 12, Issue 10, 2022.
[24] Wong C.P.Y., Coop M.R., Development of inter-particle friction in a railway ballast. Géotechnique Letters, Vol. 10, Issue 4, 2020, pp. 535-541.
[25] Guo Y., Zhang C., Xiang H., Cui G., Meng F., Zhou H., Quantitative Characterization Method for Rock Surface Roughness with Different Scale Fluctuation. KSCE Journal of Civil Engineering, Vol. 26, Issue 4, 2022, pp. 1695-1711.
[26] Wang X., Xu Y., Jackson R. L., Theoretical and Finite Element Analysis of Static Friction Between Multi-Scale Rough Surfaces. Tribology Letters, Vol. 66, 2018, pp. 1-18.
[27] Jardim P. L. G., Horowitz F., Felde N., Schröder S., Coriand L., Duparré A., Determination of the Wenzel roughness parameter by the Power Spectral Density of functional Alumina surfaces. Thin Solid Films, Vol. 606, 2016, pp. 57-62.
[28] Jacobs T. D. B., Junge T., Pastewka L., Quantitative characterization of surface topography using spectral analysis. Surface Topography: Metrology and Properties, Vol. 5, Issue 1, 2017.
[29] Kawamoto, R., Andrade, J. and Matsushima, T., A 3-D mechanics-based particle shape index for granular materials. Mechanics Research Communications, Vol. 92, 2018, pp. 67-73.
[30] Bach H., Latal C., Attrition Kinetics of the Los-Angeles-Test. Geotechnical and Geological Engineering, Vol. 41, Issue 2, 2023, pp.597-609.